

Open charm in nuclear matter at finite temperature

L. Tolós¹, A. Ramos² and T. Mizutani³

¹ Frankfurt Institute for Advanced Studies. J.W. Goethe-Universität,
Ruth-Moufang-Str. 1, 60438 Frankfurt am Main, Germany

² Departament d'Estructura i Constituents de la Matèria
Universitat de Barcelona, Diagonal 647, 08028 Barcelona, Spain

³ Department of Physics, Virginia Polytechnic Institute and State University
Blacksburg, VA 24061, USA

February 9, 2022

Abstract

We study the properties of open-charm mesons (D and \bar{D}) in nuclear matter at finite temperature within a self-consistent coupled-channel approach. The meson-baryon interactions are adopted from a type of broken SU(4) s -wave Tomozawa-Weinberg terms supplemented by an attractive scalar-isoscalar interaction. The in-medium solution at finite temperature incorporates Pauli blocking effects, mean-field binding on all the baryons involved, and π and open-charm meson self-energies in a self-consistent manner. In the DN sector, the Λ_c and Σ_c resonances, generated dynamically at 2593 MeV and 2770 MeV in free space, remain close to their free-space position while acquiring a remarkable width due to the thermal smearing of Pauli blocking as well as from the nuclear matter density effects. As a result, the D meson spectral density shows a single pronounced peak for energies close to the D meson free-space mass that broadens with increasing matter density with an extended tail particularly towards lower energies. The \bar{D} potential shows a moderate repulsive behavior coming from the dominant $I = 1$ contribution of the $\bar{D}N$ interaction. The low-density theorem is, however, not a good approximation for the \bar{D} self-energy in spite of the absence of resonance-hole contributions close to threshold in this case. We speculate the possibility of D -mesic nuclei as well as discuss some consequences for the J/Ψ suppression in heavy-ion collisions, in particular for the future CBM experiment at FAIR.

PACS: 12.38.Lg, 14.20.Lq, 14.20.Jn, 14.40.Lb, 21.65.+f, 25.80.-e

Keywords: Effective s -wave meson-baryon interaction, Coupled DN channels, Charmed mesons, Finite temperature, Spectral function, $\Lambda_c(2593)$ and $\Sigma_c(2800)$ in nuclear matter.

1 Introduction

The interest in the open and hidden charmed mesons within the context of relativistic nucleus-nucleus collisions was triggered about 20 years ago. More specifically, the suppression of the J/Ψ production was predicted as a rather clear signature of the formation of quark-gluon plasma (QGP) in ultra-relativistic central nucleus-nucleus collisions in Ref. [1]. According to its authors, a Debye-type color screening in the gluon exchanges blocks the formation of charmonium ($c\bar{c}$) bound states. Then, starting about 10 years later, the NA50 and NA60 Collaborations (see for example [2–5], in the CERN SPS fixed target experiments) actually claimed to have observed such a suppression in Pb + Pb collisions at ≈ 160 A GeV. Upon the start of the Brookhaven RHIC heavy nucleus collider a little more than 6 years ago with, say, central collision of Au + Au at $\sqrt{s_{NN}} = 200$ GeV, a new set of exciting results has gradually come out, such as an apparent energy independence of the J/Ψ suppression [6] as compared with the SPS result with $\sqrt{s_{NN}} = 17$ GeV. Firmly establishing the origin of this charmonium suppression as due to the formation of the QGP appears to need more careful analyses of the data. However, if formed in such ultra-relativistic collisions, the QGP would correspond to the one with a rather high temperature: $T > T_c$, where the critical temperature extracted from recent QCD lattice simulation [7] is $T_c \approx 175$ MeV with a low-baryon number density ρ_B (or chemical potential μ_B), supposedly similar to the situation during the initial Big-Bang period. This part of the $T - \mu_B$ phase diagram of the hadronic/partonic *matter* will continue to be the major subject of further intense activities at RHIC as well as at the CERN LHC facility (expected at $\sqrt{s_{NN}} > 5$ TeV for Pb+Pb).

Equally interesting as well as important is the somewhat complementary region of the phase diagram which is characterized by a moderate temperature but with large ρ_B . According to recent lattice simulations (see for example [8]), here a highly compressed hadronic matter gets transformed into a dense partonic matter (or strongly interacting QGP) where the boundary of the two phases is characterized by a first-order phase transition, as opposed to the above-mentioned RHIC-type hadron \leftrightarrow QGP transition which the calculation has found as a smooth cross over (see also a so-called Polyakov loop extended NJL (PNJL) approach to the subject [9]). The CBM (Compressed Baryon Matter) experiment of the FAIR project at GSI aims at investigating an important portion of this moderate T and large μ_B part of the phase diagram by a high-intensity beam of, for example, uranium nuclei of up to 35 A GeV which overlaps with the SPS energy. In this way one may expect to study possible modifications of the properties of various mesons in dense baryonic matter. In particular, since the charmed mesons produced at FAIR will not be at high energies but could be close to threshold, their medium modification may be significative. This should apply equally to the production of open-charm mesons such as D and \bar{D} as well as to hidden charmed mesons: charmonia. For the latter, one will be able to study the possible suppression and regeneration of the J/Ψ at moderate energies by mechanisms that may be of conventional hadronic origin, or due to deconfinement but different from the high T (QGP) color screening scheme proposed in [1] and being sought by the far higher energy RHIC accelerator, as stated earlier.

Our present interest is in relativistic heavy-ion collisions which fit into some part of the domain of the phase diagram covered by the FAIR project. In particular, we would like to focus on hadronic approaches to the in-medium modification of the $D(\bar{D})$ mesons which may

- (i) enter the explanation of the possible J/Ψ suppression in relativistic nucleus-nucleus collisions, see for example Ref. [10], with special interest in the FAIR energies.
- (ii) provide a theoretical support for an anticipated open-charm enhancement again within the FAIR energies [11], an issue that was triggered by the NA50 Collaboration, but was not recognized by the NA60 result, see [12].
- (iii) infer possible D^0, D^-, \bar{D}^0 bound states in heavy nuclei such as Pb [13].

Here we should stress that all these interpretations/predictions are based upon the possible attraction felt by the $D(\bar{D})$ mesons which could lead to their mass reduction in the nuclear medium [13–16]. For example, within these mostly hadronic pictures, the J/Ψ absorption by collision with nucleons and mesons was suggested to take place at little or no extra cost of energy due to the lowering of the threshold for $D\bar{D}$ pairs, facilitating reactions of the J/Ψ with comoving mesons, such as $J/\Psi\pi \rightarrow D\bar{D}$. In a similar manner, processes such as $J/\Psi N \rightarrow \bar{D}Y_c$ where Y_c is one of the charmed baryons may proceed more easily. A critical and detailed review on these *mean field* approaches was made in [17] which eventually points to the necessity of performing a coupled-channels meson-baryon scattering in nuclear medium due to strong coupling among the DN and other meson-baryon channels with same quantum numbers. Hence, in the present article, we pursue a coupled-channel study on the spectral properties of the open-charm D and \bar{D} mesons in nuclear matter at finite temperatures. In this regard, we want to remark that kinetic equilibrium assumed in the corresponding heavy-ion reactions to introduce a well-defined temperature may yet to be firmly established, although, as pointed out in [11], non-equilibrium transport equation methods appear to support the thermalization picture [18–20] at SPS energies. To set the basis, we should mention here earlier prototypes to the present study. First, a coupled-channel approach based on a set of separable meson-baryon interactions was adopted with an underlying $SU(3)$ symmetry among the $u-, d-, c-$ quarks (thus excluding the strangeness related channels). After model parameters were fixed to reproduce the position and width of the $\Lambda_c(2593)$, it was applied to study the in-medium spectral function of the D meson for a zero temperature nuclear matter environment [21]. This was later extended to finite temperatures [22]. Next, based upon a $SU(4)$ scheme broken by the masses of the exchanged vector mesons (the charmed ones in particular), hence including also the channels with strangeness [23], an effective meson-baryon interaction, of lowest order in both chiral and heavy-quark symmetries, was introduced to study the D mesons in nuclear matter at zero temperature [17, 24].

To continue and complete this sequence, in the present article we are extending the result of Ref. [17] to study the D and \bar{D} mesons in nuclear matter of up to twice the normal density, and having a temperature from zero up to 150 MeV. A couple of extra additions in the present work include: (a) an explicit consideration of the nuclear mean-field binding effect on all the baryons involved in the coupled channels, inclusive of strange and charmed, and (b) the study of the in-medium \bar{D} (note that [24] also looked at this aspect).

Equipped with those tools and ingredients, we go beyond the result of Refs. [13–16] and try to determine the continuous in-medium spectral (or *mass*) distribution of D and \bar{D} , and show that the former deviates significantly from the delta-function type spike at the free-space mass or at the value shifted to elsewhere. Also we obtain optical potentials for D and \bar{D} . These are important ameliorations in view of the points (i)–(iii) stated above.

The organization of the present article goes as follows: in Sect. 2 we develop the formalism and ingredients on which the calculation in the present work is based. Sect. 3 is devoted to the presentation and discussion of the results. Finally, in Sect. 4 we draw our conclusions and give final remarks pertaining to the present and future works.

2 Open-charm mesons in nuclear matter at finite temperature

Our objective in this section is to obtain the D and \bar{D} in-medium self-energy by solving the corresponding multi-channel T matrix equation. Then, the obtained self-energy is used to find the $D(\bar{D})$ spectral function in an iso-symmetric nuclear matter at finite temperature. This is done by extending the procedure found in Ref. [17] to a non-zero temperature environment by the procedure adopted in Ref. [22]. As mentioned in Sect. 1, we shall also introduce the binding effect to all the baryons involved by the nuclear matter mean field.

2.1 Coupled meson-baryon channels in free space

The first step towards our goal is to obtain the free space T -matrices for the coupled meson-baryon system involving $DN(\bar{D}N)$. We shall briefly summarize it as discussed in Ref. [17]. These matrices follow the standard multi-channel scattering (integral) equation,

$$T = V + VGT, \quad (1)$$

where V is a symmetric matrix consisting of a set of meson-baryon transition interactions (potentials). They are obtained from the tree level s -wave contribution to the meson-baryon scattering, and will be specified later. As shown in Ref. [25, 26], the kernel of the equation for s -wave interaction can be factorized in the on-mass-shell ansatz, leaving the four-momentum integration only in the two-particle meson-baryon propagators. These quantities often called loop functions form a diagonal matrix G . They are divergent and thus need to be regularized. In the present work the cut-off method is adopted as it is more appropriate than dimensional methods when dealing with particles in a medium, as done in Refs. [27, 28] where it is applied in the study of \bar{K} in nuclear matter.

The consequence of the on-shell ansatz is a set of linear algebraic equations whose solution now reads,

$$T = [1 - VG]^{-1}V, \quad (2)$$

which is practically equivalent to the so-called N/D method [25].

The meson-baryon transition interaction V is characterized here by the channel quantum numbers, charm C , strangeness S and isospin I . We implicitly fix the first two quantum numbers and label V explicitly by I . For each (C, S) fixed, the coupled-channel elements of the symmetric matrix V of a given isospin I are specified as V_{ij}^I for a transition $i \leftrightarrow j$. For $(C = 1, S = 0)$, i and j run through

$\pi\Sigma_c(2589)$, $DN(2810)$, $\eta\Lambda_c(2835)$, $K\Xi_c(2960)$, $K\Xi'_c(3071)$, $D_s\Lambda(3085)$ and $\eta'\Lambda_c(3245)$ for the $I = 0$ sector, and

$\pi\Lambda_c(2425)$, $\pi\Sigma_c(2589)$, $DN(2810)$, $K\Xi_c(2960)$, $\eta\Sigma_c(3005)$, $K\Xi'_c(3071)$, $D_s\Sigma(3160)$ and $\eta'\Sigma_c(3415)$

for the $I = 1$ sector. In the case $(C = -1, S = 0)$, there is only a single channel, $\bar{D}N(2810)$, for each isospin $I = 0$ and $I = 1$ value. We note that, in the above description, the value in the parentheses denotes the channel threshold in MeV.

The concrete form for the matrix elements of V comes from the s -wave Tomozawa-Weinberg (T-W) term as the zero-range limit of the lowest-order interaction of the SU(4) pseudoscalar meson and $1/2^+$ ground-state baryon multiplets based on the universal vector-meson coupling hypothesis equipped with the extended KSFR condition (see Ref. [17] for details):

$$V_{ij}^I(\sqrt{s}) = -\frac{\kappa C_{ij}}{4f^2} (2\sqrt{s} - M_i - M_j) \left(\frac{M_i + E_i}{2M_i} \right)^{1/2} \left(\frac{M_j + E_j}{2M_j} \right)^{1/2}. \quad (3)$$

The coupling strength C_{ij} derives from the SU(4) symmetry for the $i \leftrightarrow j$ transition, \sqrt{s} is the center of mass energy, $f = 1.15 f_\pi$, where the value of f has been adopted from Ref. [26], and M_i and M_j as well as E_i and E_j are the masses and energies of baryons in channels i and j , respectively. The breaking of the SU(4) symmetry in the T-W interaction through the physical hadron masses is mostly eminent in the reduction factor κ which is *unity* for transitions $i \leftrightarrow j$, driven by uncharmed vector-meson exchanges (ρ , ω , ϕ , K^*) but is equal to $\kappa_c = (\bar{m}_V/\bar{m}_V^c)^2 \approx 1/4$ for charmed vector-meson exchanges such as D^* and D_s^* , where $\bar{m}_V(\bar{m}_V^c)$ is the mass of the typical uncharmed (charmed) exchanged vector meson. The transition coefficients $\tilde{C}_{ij} \equiv \kappa C_{ij}$, which are symmetric with respect to the indices, are listed in Tables I and II of Ref. [17] for the DN sector. For the $\bar{D}N$ system, $\tilde{C}_{\bar{D}N \rightarrow \bar{D}N}^{I=0} = 0$ and $\tilde{C}_{\bar{D}N \rightarrow \bar{D}N}^{I=1} = -2$. The reader is reminded of the same situation for the KN coupling strengths due to SU(3) symmetry. The T-W vector interaction is supplemented by a scalar-isoscalar attraction, which turns out to be important in kaon condensate studies (see Ref. [16, 29]). The s -wave projection of this interaction is equal to

$$V_\Sigma(\sqrt{s}) = -\frac{\Sigma_{DN}}{f_D^2} \left(\frac{M_N + E}{2M_N} \right), \quad (4)$$

and it is independent of the C and I specification in the present context. Here, f_D is the $D(\bar{D})$ meson weak decay constant, and Σ_{DN} is the strength of this interaction. Note that for simplicity we introduce this only in the diagonal $D(\bar{D})N$ interaction. The most recent determination of $f_D = 157$ MeV may be found in [30]. As for the value of Σ_{DN} , we simply follow what a QCD sum-rule [15] and a nuclear mean-field approach of [16] have

suggested, and estimate it conservatively as $\Sigma_{DN} \approx 2000$ MeV. Because we can only aim at qualitative estimates, we set $f_D \sim 200$ MeV and determine the strength of the scalar-isoscalar interaction to be $\Sigma = \Sigma_{DN}/f_D^2 = 0.05$ MeV $^{-1}$. We also accommodate the case where no such attraction is added, hence $\Sigma_{DN} = 0$. Based upon the above interactions, the multi-channel transition T matrices are solved such that the momentum cut-off Λ is fixed to reproduce the position and the width of the $I = 0$ $\Lambda_c(2593)$ resonance. The parameters for the two cases adopted from [17] are used in the present work, model A: $f = 1.15f_\pi$, $\Sigma = 0.05$ MeV $^{-1}$, $\Lambda = 727$ MeV, and model B: $f = 1.15f_\pi$, $\Sigma = 0$ MeV $^{-1}$, $\Lambda = 787$ MeV. These two model interactions produce a resonance in $I = 1$ channel whose position and width are: 2770 MeV, 20 MeV (model A), and 2795 MeV, 20 MeV (model B), respectively, close to the nominal $\Sigma_c(2800)$ [31].

2.2 Coupled meson-baryon interaction in finite-temperature nuclear matter with mean-field binding

The properties of the $D(\bar{D})$ mesons in nuclear matter at finite temperature and with mean-field binding are obtained by incorporating the corresponding medium modifications in the loop function matrix G only. That is, we assume that the interaction matrix V stays unchanged in medium. In Eq. (3), the two square rooted factors come from the baryon spinor normalization, hence should stay more or less the same. The finite-temperature nuclear mean-field binding makes the in-medium baryon masses $M_i^*(T)$ to be shifted from their free space values M_i , so the second factor in the expression should be different in medium. We nevertheless retain the vacuum mass values in this interaction as we have estimated the effect to be at most a few percent in magnitude. For the same reason the scalar-isoscalar interaction Eq. (4) remains unchanged. By implicitly understanding that G and T are now to be interpreted as medium modified, the same multi-channel algebraic equation Eq. (2) is to be solved.

Let us now describe in detail the medium and temperature modifications. First, the baryons in the coupled channels, namely the nucleon, Λ , Σ , Λ_c and Σ_c , change both their mass and energy-momentum relations due to the finite-temperature mean-field binding effect. We have adopted a temperature dependent Walecka-type $\sigma - \omega$ model to account for this change, see for example Ref. [32]. Within this model, the nucleon energy spectrum in mean-field approximation is obtained from

$$E_N(\vec{p}, T) = \sqrt{\vec{p}^2 + M_N^*(T)^2} + \Sigma^v, \quad (5)$$

with the vector potential Σ^v and the effective mass $M_N^*(T)$ given by

$$\begin{aligned} \Sigma^v &= \left(\frac{g_v}{m_v} \right)^2 \rho \\ M_N^*(T) &= M_N - \Sigma^s, \quad \text{with } \Sigma^s = \left(\frac{g_s}{m_s} \right)^2 \rho_s, \end{aligned} \quad (6)$$

where m_s and m_v are the meson masses, while g_s and g_v are the density dependent scalar and vector coupling constants, respectively. These constants are obtained by reproducing

the energy per particle of symmetric nuclear matter at $T = 0$ coming from a Dirac-Brueckner-Hartree-Fock calculation (see Table 10.9 of Ref. [33]). The *ordinary* nuclear matter (Lorentz) vector density (ρ) and (Lorentz) scalar density (ρ_s) are obtained from the corresponding vector ($n(\vec{p}, T)$) and scalar ($n_s(\vec{p}, T)$) density distributions defined in terms of the Fermi-Dirac function as

$$n(\vec{p}, T) = \frac{1}{1 + \exp[(E_N(\vec{p}, T) - \mu)/T]}, \quad n_s(\vec{p}, T) = \frac{M^*(T)n(\vec{p}, T)}{\sqrt{\vec{p}^2 + M^*(T)^2}}, \quad (7)$$

by momentum integration, namely

$$\rho = \frac{4}{(2\pi)^3} \int d^3p \, n(\vec{p}, T) \quad (8)$$

(and similarly for ρ_s). As may be clear from the above development, $E_N(\vec{p}, T)$, $M_N^*(T)$ and the chemical potential μ are obtained simultaneously and self-consistently for given ρ and for the corresponding values of g_s and g_v . The values of the nucleon scalar and vector potentials in nuclear matter at $\rho_0 = 0.16 \text{ fm}^{-3}$ and at $T = 0$ are $\Sigma^s = 356 \text{ MeV}$ and $\Sigma^v = 278 \text{ MeV}$.

The hyperon (Y) as well as the charmed baryon (Y_c) masses and energy spectra can be easily inferred from those for the nucleon as

$$E_{Y(c)}(\vec{p}, T) = \sqrt{\vec{p}^2 + M_{Y(c)}^*(T)^2} + \Sigma_{Y(c)}^v, \quad (9)$$

where

$$\begin{aligned} \Sigma_{Y(c)}^v &= \frac{2}{3} \left(\frac{g_v}{m_v} \right)^2 \rho = \frac{2}{3} \Sigma^v, \\ M_{Y(c)}^*(T) &= M_{Y(c)} - \Sigma_{Y(c)}^s = M_{Y(c)} - \frac{2}{3} \left(\frac{g_s}{m_s} \right)^2 \rho_s \\ &= M_{Y(c)} - \frac{2}{3} (M_N - M_N^*(T)). \end{aligned} \quad (10)$$

Here we have assumed that the σ and ω fields only couple to the u and d quarks, as in Ref. [34], so the scalar and vector coupling constants for hyperons and charmed baryons are:

$$g_v^{Y(c)} = \frac{2}{3} g_v, \quad g_s^{Y(c)} = \frac{2}{3} g_s. \quad (11)$$

We note that the quark-meson coupling (QMC) calculations of Ref. [34], performed at $T = 0$, obtained a somewhat smaller scalar potential (about half the present one) for the $\Lambda_{(c)}$ and $\Sigma_{(c)}$ baryons due to the inclusion of an effective coupling for each baryon species, $C_j(\tilde{\sigma})$, where “j” is the label for baryons. This factor was introduced to mimic the baryon structure. To the best of our knowledge, no temperature effects have been studied within this framework.

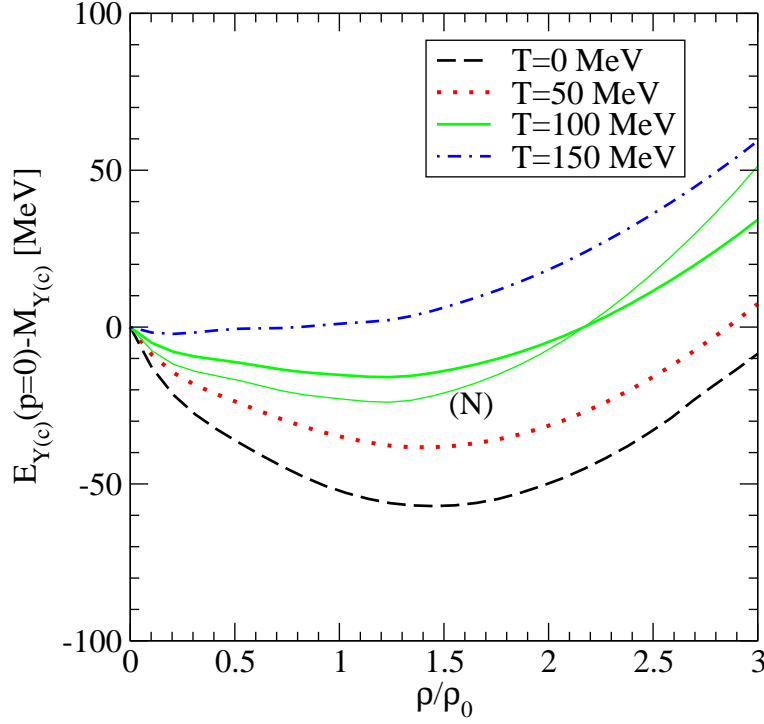


Figure 1: The potential at zero momentum for the hyperons ($Y = \Lambda, \Sigma$) and charmed baryons ($Y_c = \Lambda_c, \Sigma_c$) as a function of the density for different temperatures. The thin solid line displays the nucleon potential at $T = 100$ MeV.

The potential at zero momentum $V = E_{Y(c)}(\vec{p} = 0) - M_{Y(c)}$ for different baryon species obtained in the present work is shown in Fig. 1 as a function of the density for different temperatures. Obviously, the potential for hyperons and charmed baryons follows the simple light quark counting rule as compared with the nucleon potential: $V_{Y(c)} = 2/3V_N$. The attraction at $\rho = \rho_0$ and $T = 0$ MeV is about -50 MeV, the size of which gets reduced as temperature increases turning even into repulsion, especially at higher densities. This behavior results from the fact that the temperature independent vector potential takes over the strongly temperature-dependent scalar potential which decreases with temperature.

The second medium effect is the Pauli exclusion principle acting on the nucleon in the intermediate $D(\bar{D})N$ loop function. This is implemented by replacing the single free-nucleon propagator in the loop function by the corresponding in-medium one:

$$G_N(p_0, \vec{p}, T) = \frac{1 - n(\vec{p}, T)}{p_0 - E_N(\vec{p}, T) + i\varepsilon} + \frac{n(\vec{p}, T)}{p_0 - E_N(\vec{p}, T) - i\varepsilon}, \quad (12)$$

where the effect of the temperature is contained in the nucleon Fermi-Dirac distributions and single-particle energies.

The third medium effect is the dressing of the mesons, due to their interactions with the surrounding nucleons in the course of propagating through nuclear matter. In particular,

we will consider the dressing of pions and $D(\bar{D})$ mesons. The reason for not doing so for other mesons will be stated below.

The meson dressing is represented by the in-medium meson self-energy $\Pi_i(q_0, \vec{q}, T)$, where $i = D, \bar{D}, \pi$ in the present case. This quantity appears in the corresponding in-medium single meson propagator:

$$D_i(q_0, \vec{q}, T) = \frac{1}{q_0^2 - \vec{q}^2 - m_i^2 - \Pi_i(q_0, \vec{q}, T)} . \quad (13)$$

In the Lehmann integral representation, the meson propagator may be expressed in terms of the spectral function $S_i(q_0, \vec{q}, T)$ as

$$D_i(q_0, \vec{q}, T) = \int_0^\infty \frac{S_i(\omega, \vec{q}, T)}{q_0 - \omega + i\varepsilon} d\omega - \int_0^\infty \frac{S_{\bar{i}}(\omega, \vec{q}, T)}{q_0 + \omega - i\varepsilon} d\omega, \quad (14)$$

where \bar{i} is the anti-particle to meson i . Then we easily relate the self-energy and spectral function as

$$S_i(q_0, \vec{q}, T) = -\frac{1}{\pi} \text{Im} D_i(q_0, \vec{q}, T) = -\frac{1}{\pi} \frac{\text{Im} \Pi_i(q_0, \vec{q}, T)}{|q_0^2 - \vec{q}^2 - m_i^2 - \Pi_i(q_0, \vec{q}, T)|^2} . \quad (15)$$

For the case of pions, we incorporate the self-energy at finite temperature given in the Appendix of Ref. [35], which was obtained by incorporating the thermal effects to the $T = 0$ pion self-energy model given, for instance, in Refs. [36, 37]. We recall that the pion self-energy in nuclear matter at $T = 0$ was obtained by adding to a small repulsive and constant s -wave part [38], the p -wave contribution coming from the coupling to $1p$ - $1h$, 1Δ - $1h$ and $2p$ - $2h$ excitations together with short-range correlations. These correlations are mimicked by the Landau-Migdal parameter g' , taken from the particle-hole interaction described in Ref. [39], which includes π and ρ exchanges modulated by the effect of nuclear short-range correlations.

In the case of the $D(\bar{D})$ mesons, the self-energy is obtained self-consistently from the s -wave contribution to the in-medium $D(\bar{D})N$ amplitude, as will be shown explicitly at the end of this section.

With these medium modifications the propagator loop functions are obtained by four-momentum convolution of meson and baryon single-particle propagators:

$$G_{D(\bar{D})N}(P_0, \vec{P}, T) = \int \frac{d^3q}{(2\pi)^3} \frac{M_N}{E_N(\vec{P} - \vec{q}, T)} \times \left[\int_0^\infty d\omega S_{D(\bar{D})}(\omega, \vec{q}, T) \frac{1 - n(\vec{P} - \vec{q}, T)}{P_0 - \omega - E_N(\vec{P} - \vec{q}, T) + i\varepsilon} + \int_0^\infty d\omega S_{\bar{D}(D)}(\omega, \vec{q}, T) \frac{n(\vec{P} - \vec{q}, T)}{P_0 + \omega - E_N(\vec{P} - \vec{q}, T) - i\varepsilon} \right], \quad (16)$$

for $D(\bar{D})N$ states and

$$G_{\pi Y_c}(P_0, \vec{P}, T) = \int \frac{d^3 q}{(2\pi)^3} \frac{M_{Y_c}}{E_{Y_c}(\vec{P} - \vec{q}, T)} \int_0^\infty d\omega S_\pi(\omega, \vec{q}, T) \times \frac{1 + n_\pi(\vec{q}, T)}{P_0 - \omega - E_{Y_c}(\vec{P} - \vec{q}, T) + i\epsilon} , \quad (17)$$

for $\pi\Lambda_c$ or $\pi\Sigma_c$ states, where $P = (P_0, \vec{P})$ is the total two-particle four momentum and \vec{q} is the meson momentum in the nuclear matter rest frame. Note that, for the DN loop function, the $S_{\bar{D}}(\omega, \vec{q})$ spectral function appearing in the subdominant second term on the r.h.s. of Eq. (16) is assumed to be a free-space delta function. The $\pi Y_{(c)}$ loop function incorporates the $1 + n_\pi(\vec{q}, T)$ term, with $n_\pi(\vec{q}, T)$ being the Bose distribution of pions at temperature T , in order to account for the contribution from thermal pions at finite temperature. Note that, by assuming perfect isospin symmetry, we set the pion chemical potential to zero in $n_\pi(\vec{q}, T)$.

For $\eta(\eta')Y_c$, $K\Xi_c(\Xi'_c)$ and $D_s Y$ states, the corresponding meson lines (propagators) are not dressed by self-energy insertions. In the case of the η, η' mesons, this is a reasonable approximation, because the coefficients coupling the $\eta(\eta')Y_c$ channels with the DN channel are small (see Tables I and II in Ref. [17]). Containing an \bar{s} -quark, the K couples weakly to nucleons, and its spectral function may be approximated by the free space one, viz. by a delta function. We could include a moderate repulsive in-medium shift to the kaon mass, consistent with the repulsion predicted by a $T\rho$ approximation or more sophisticated models [40], but our results are insensitive to this shift due to the zero couplings of these channels to DN . As for the spectral function of the D_s^+ meson appearing in the in-medium $D_s Y$ channels, it has been shown [24] that, in addition to the quasi-particle peak, it presents a lower energy mode associated with an exotic resonance predicted around 75 MeV below the $D_s^+ N$ threshold [23]. Therefore, with large coupling coefficients for transitions $DN \leftrightarrow D_s Y$, one may eventually have to solve an extended in-medium self-consistent coupled-channel problem combining the $C = 1, S = 0$ (DN) and $C = 1, S = 1$ ($D_s N$) sectors. Work along this line is in progress.

Lastly, we state that the in-medium $D(\bar{D})$ self energy is obtained by integrating $T_{D(\bar{D})N}$ over the Fermi distribution for nucleon momentum at a given temperature as

$$\Pi_{D(\bar{D})}(q_0, \vec{q}, T) = \int \frac{d^3 p}{(2\pi)^3} n(\vec{p}, T) [T_{D(\bar{D})N}^{(I=0)}(P_0, \vec{P}, T) + 3T_{D(\bar{D})N}^{(I=1)}(P_0, \vec{P}, T)] , \quad (18)$$

where $P_0 = q_0 + E_N(\vec{p}, T)$ and $\vec{P} = \vec{q} + \vec{p}$ are the total energy and momentum of the $D(\bar{D})N$ pair in the nuclear matter rest frame and the values (q_0, \vec{q}) stand for the energy and momentum of the $D(\bar{D})$ meson also in this frame. Recall that $\Pi_{D(\bar{D})}(q_0, \vec{q}, T)$ must be determined self-consistently since it is obtained from the in-medium amplitude $T_{D(\bar{D})N}$ which contains the $D(\bar{D})N$ loop function $G_{D(\bar{D})N}$, and this last quantity itself is a function of $\Pi_{D(\bar{D})}(q_0, \vec{q}, T)$. From this we obtain the corresponding spectral function to complete the integral for the loop function $G_{D(\bar{D})N}(P_0, \vec{P}, T)$ as in Eq. (16).

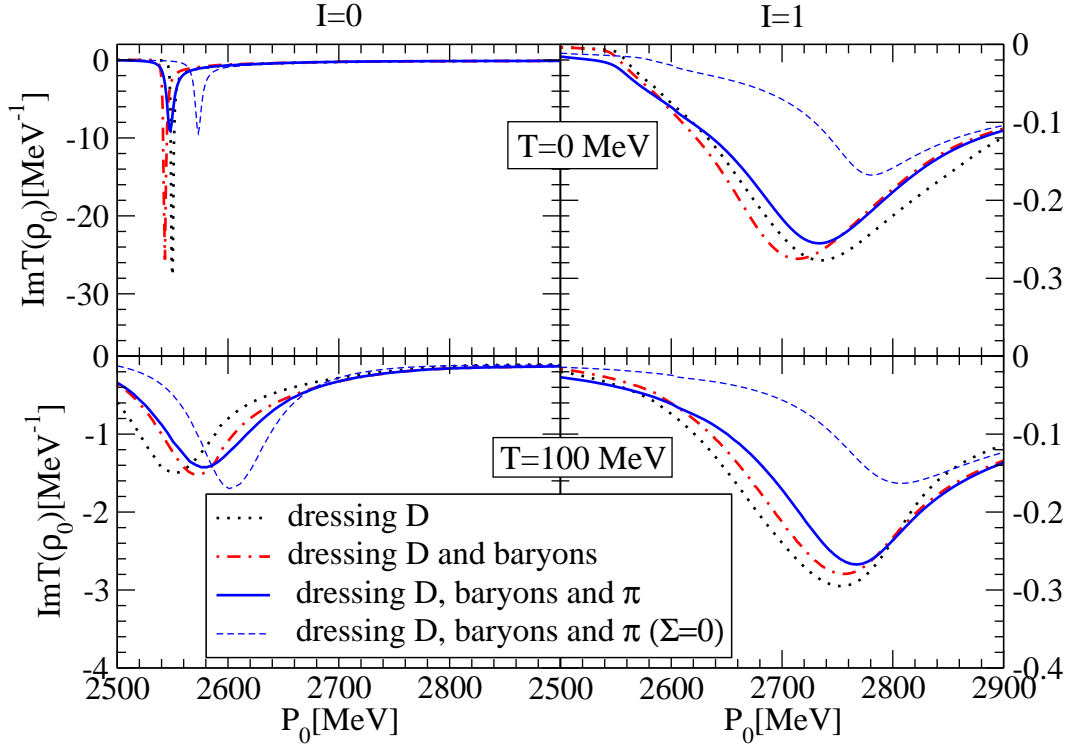


Figure 2: Imaginary part of the in-medium interaction for $I = 0$ and $I = 1$ at ρ_0 as a function of the center-of-mass energy P_0 for $T = 0$ MeV and $T = 100$ MeV, and for three different approaches in the self-consistent calculation of the D meson self-energy: i) including only the self-consistent dressing of the D meson, ii) adding the binding of the different baryons in the intermediate states and iii) including the baryon binding effects and the pion self-energy.

3 Results and Discussion

3.1 The D meson spectral function in a hot nuclear medium

We start this section by looking at the in-medium behavior of the $I = 0$ Λ_c and $I = 1$ Σ_c resonances, which in the full model of Ref. [17], appear at 2593 MeV and 2770 MeV respectively, in free space. This is summarized in Fig. 2 by the imaginary part of the in-medium $T(DN \rightarrow DN)$ matrix at saturation density $\rho_0 = 0.17 \text{ fm}^{-3}$ for $I = 0$ (left column) and $I = 1$ (right column) as a function of the center of mass energy P_0 for temperatures $T = 0$ (first row) and $T = 100$ MeV (second row), respectively. For each of the four figures, three different lines represent self-consistent calculations with increasing sophistications, viz. (i) the self-consistent dressing of D mesons only (dotted lines), (ii) D meson dressing with the inclusion of *mean-field binding effect* (MFB) on baryons in the loop functions (dash-dotted lines), and (iii) D meson dressing with the inclusion of both baryon binding

effects and *pion dressing* (PD) in the loop functions (solid lines). In the figures, the thick lines correspond to model A (viz. $\Sigma_{DN} \neq 0$) while the thin dashed lines refer to the result only for Case (iii) within model B ($\Sigma_{DN} = 0$). Recall that our principal interest is in model A. Comparison of those two model results will be found later in this section.

Our discussion is first for the zero temperature ($T = 0$) case. We begin by comparing the two first cases. We recall that medium effects (excluding baryon binding potentials) lowered the position of the Λ_c and Σ_c resonances with respect to their free-space values [17]. When baryon binding effects are incorporated, these resonances get even more lowered, as can be seen by comparing the dotted and dash-dotted lines in Fig. 2. If we had a mere attractive shift of the nucleon mass of around 75 MeV (the value of the optical potential at zero momentum) in a DN single-channel (non-self-consistent) calculation, we would be expecting the same shift in the corresponding MFB amplitude. The fact that the attractive shifts induced by MFB effects are of only 6 MeV and 22 MeV for the in-medium Λ_c resonance (hereafter denoted as $\tilde{\Lambda}_c$) and Σ_c (denoted as $\tilde{\Sigma}_c$) respectively, indicates that coupled-channel effects, momentum dependence of the binding potentials, and self-consistency play crucial roles in the determination of the in-medium DN amplitudes.

The widths of both resonances differ according to the phase space available. For the $I = 0$ sector, the lowest threshold in free space is from the $\pi\Sigma_c$ channel which lies slightly below the $\Lambda_c(2593)$ resonance position, and constrains this resonance to be narrow. This is also the case in nuclear matter. This narrowness is somewhat relaxed by the processes $\tilde{\Lambda}_c N \rightarrow \pi N \Lambda_c, \pi N \Sigma_c$, which open up in medium through the D meson self-energy. The $I = 1$ $\tilde{\Sigma}_c$ resonance, which shows a free-space width of 30 MeV [17], develops a large width of the order of 200 MeV, due to the opening of new absorption processes of the type $\tilde{\Sigma}_c N \rightarrow \pi N \Lambda_c, \pi N \Sigma_c$, which is similar to the case of the $\tilde{\Lambda}_c$ but has a much larger decaying phase space.

As for the effect of pion dressing (PD) implemented in Case (iii), we expected it to be of minor importance in the present approach, in contrast to the findings in [27, 35] for $\bar{K}N$ amplitude in nuclear matter, and also in Ref. [21, 22] for in-medium DN . This is due to the reduction factor $\kappa_c \approx 1/4$ in the $DN \leftrightarrow \pi Y_c$ transition (see Eq.(3)) due to the charm transfer as shown in Ref. [17]. Still a small effect is seen in the positions and widths of the \tilde{Y}_c ($= \tilde{\Lambda}_c, \tilde{\Sigma}_c$) through the absorption of these resonances by one and two nucleon processes ($\tilde{Y}_c N \rightarrow Y_c N$ and $\tilde{Y}_c NN \rightarrow Y_c NN$), which open up through the $1p - 1h$ and $2p - 2h$ components of the pion self-energy.

With regard to the results for models A and B, we observe that both models are qualitatively similar. However, the absence of the Σ_{DN} term in model B produces in-medium resonances at higher energies, therefore the corresponding widths are larger due to the increased decaying phase space. As compared with their free-space resonance positions, the $\tilde{\Lambda}_c$ lies 45 MeV lower and the $\tilde{\Sigma}_c$ is at 40 MeV below the free value for model A. In model B, the $\tilde{\Lambda}_c$ lies 20 MeV lower while the $\tilde{\Sigma}_c$ moves up roughly by 10 MeV. These results are consistent with those obtained in Ref. [17] where mean-field baryon binding is absent. In the case of the $I = 1$ amplitude, the attraction provided by a self-consistent calculation using model B is not enough to fully compensate the repulsion induced by Pauli blocking effects.

Now we come to the finite temperature case. The overall effects from $T \neq 0$ result is the reduction of the Pauli blocking factor since the Fermi surface is smeared out with temperature. Therefore, both resonances move up in energy to get closer to their position in free space while they are smoothen out. The inclusion of MFB (viz. Case (ii)) for $T = 100$ MeV induces a shift of both resonances to higher energies, opposite to what is found for $T = 0$, hence it appears counter intuitive. The reason behind this is that the potential of each baryon from MFB becomes less attractive with increasing temperature and also with increasing momentum (see Fig. 1 for evolution in temperature of the baryonic potentials at zero momentum). At a high enough value of temperature, the single-particle potential may become repulsive already at a relatively low momentum. It will then become more difficult to excite intermediate states if they carry a repulsive potential and, consequently, the resonance will be generated at higher energies than in the absence of MFB effects, as is already the case at $T = 100$ MeV and $\rho = \rho_0$. Again, the PD does not drastically alter the resonance positions. At $T = 100$ MeV, $\tilde{\Lambda}_c$ is at 2579 MeV for model A and $\tilde{\Sigma}_c$ at 2767 MeV, while model B generates both resonances at higher energies: $\tilde{\Lambda}_c$ at 2602 MeV and $\tilde{\Sigma}_c$ at 2807 MeV. The spreading of the resonant structures in T_{DN} with increasing temperature has an important bearing in the temperature dependence of the D meson spectral function as we shall discuss below.

In Fig. 3 we display the D meson spectral function at zero momentum and normal saturation density ρ_0 for two distinct values of temperature: $T = 0$ and $T = 100$ MeV, and for Cases (i) to (iii) (thick lines) for model A. As in the previous figure, we only show the result from Case (iii) for model B with thin-dashed lines.

At $T = 0$ the spectral function presents two peaks: the one at lower energy is built up from the $\tilde{\Lambda}_c N^{-1}$ excitation, whereas the second one at higher energy is mainly driven by the quasi(D)-particle peak but mixes considerably with the $\tilde{\Sigma}_c N^{-1}$ state. The quasiparticle energy $E_{qp}(\vec{q})$ may be found from the solution of $\text{Re} [D_D(q_0, \vec{q}, T)]^{-1} = 0$ for q_0 , hence

$$E_{qp}(\vec{q})^2 = \vec{q}^2 + m_D^2 + \text{Re} \Pi_D(E_{qp}(\vec{q}), \vec{q}) . \quad (19)$$

We observe that, once MFB is included (Case (ii)), the lower peak in the spectral function due to the $\tilde{\Lambda}_c N^{-1}$ mode goes up by about 50 MeV relative to the Case (i) result. This could be understood in the following manner: as seen in Fig. 2, the $\tilde{\Lambda}_c$ resonance moves to lower energies by about 6 MeV upon going from Case (i) to Case (ii), but at the same time the nucleon energy goes down due to MFB, hence the peak in the D meson spectral function goes up as the $\tilde{\Lambda}_c N^{-1}$ excitation effectively costs more energy. In other words, the meson requires to carry more energy to compensate for the attraction felt by the nucleon. The same characteristic feature is seen also for the $\tilde{\Sigma}_c N^{-1}$ configuration that mixes with the quasiparticle peak. Just in line with the in-medium T_{DN} amplitude studied earlier (Fig. 2), the PD installed in Case (iii) does not alter much the position of $\tilde{\Lambda}_c N^{-1}$ excitation or the quasiparticle peak. From Eq. (19), the corresponding quasiparticle energy is found at 1855 MeV, i.e. lower than the free mass by 12 MeV. However, the actual peak appears slightly shifted upwards due to the energy dependence of the imaginary part of the D meson self-energy affected by the $\tilde{\Sigma}_c N^{-1}$ configuration. For model B (Case iii only), the absence of

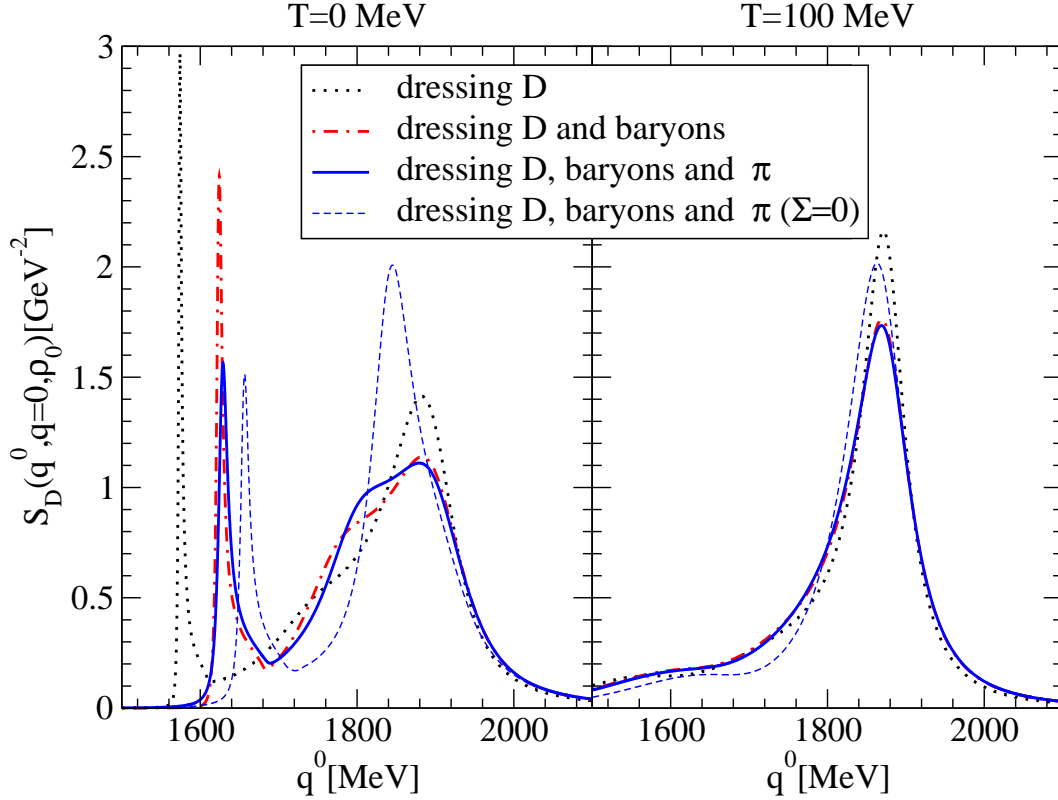


Figure 3: The zero-momentum D meson spectral function at $\rho = \rho_0$ for $T = 0$ MeV and $T = 100$ MeV as a function of the D meson energy for the previous approaches.

the Σ_{DN} term moves the $\tilde{\Lambda}_c N^{-1}$ excitation closer to the quasiparticle peak, while the latter fully mixes with the $\tilde{\Sigma}_c N^{-1}$ excitation.

When the finite temperature effects are included (see the right-hand side of Fig. 3 for $T = 100$ MeV), the quasiparticle peak of the spectral function at zero momentum is found to move closer to the free-space mass value due to the smearing of the nuclear matter Fermi surface. The reason is that the self-energy receives contributions from higher momentum DN pairs that feel a weaker interaction. Furthermore, structures from the $\tilde{Y}_c N^{-1}$ modes seen at $T = 0$ are smeared out with increasing temperature, an effect that was reported earlier in Ref. [22]. Eventually, at $T = 100$ MeV we are left with a quasiparticle peak at 1869 MeV (model A) and 1863 MeV (model B), amazingly close to the free space mass, $M(D) = 1867$ MeV, but with a large width due to collisional broadening. Again, due to the energy dependence of the self-energy, the positions of these peaks differ slightly from the value of the quasiparticle energies of 1864 MeV and 1861 MeV, respectively. The slow fall-off on the left-hand side of the quasiparticle peak corresponds mostly to the diluted $\tilde{\Lambda}_c N^{-1}$ configuration.

The evolution of the spectral function as a function of temperature is presented in Fig. 4 for two different densities, ρ_0 and $2\rho_0$, and two momenta, $q = 0$ MeV/c and $q = 450$ MeV/c,

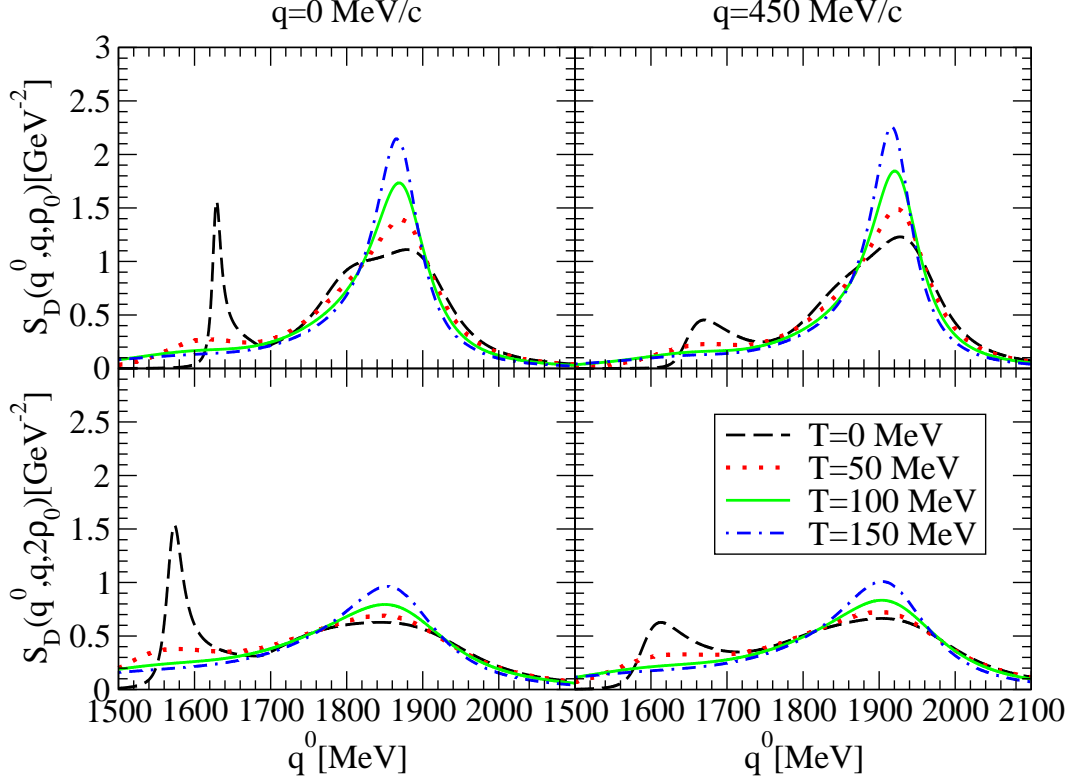


Figure 4: The D meson spectral function for $q = 0$ MeV/c and $q = 450$ MeV/c at ρ_0 and $2\rho_0$ as a function of the D meson energy for different temperatures and for the self-consistent calculation including the dressing of baryons and pions in model A ($\Sigma_{DN} \neq 0$).

in the full self-consistent calculation (Case (iii)) for model A. As already mentioned before, we observe the dilution of the $\tilde{\Lambda}_c N^{-1}$ and $\tilde{\Sigma}_c N^{-1}$ structures with increasing temperature, while the quasiparticle peak gets closer to its free value and it becomes narrower. The widening of the quasiparticle peak for larger nuclear density may be understood as due to the enhancement of collision and absorption processes. As a result, the quasiparticle peak position is difficult to extract directly from the plot at high densities. As for the structure in the lower values of q_0 due to the $\tilde{\Lambda}_c N^{-1}$ configuration, it moves down with increasing nuclear matter density due to the lowering in the position of the $\tilde{\Lambda}_c$ resonance induced by the more attractive Σ_{DN} term, as based on our experience in Ref. [17]. Then by picking up the case with $q = 0$, $\rho = \rho_0$ (upper left-hand panel in Fig. 4) as an example, we want to analyze the behavior of the same structure as a function of T . This $\tilde{\Lambda}_c N^{-1}$ particle-hole configuration evolves from a sharp/narrow peak with very little strength below $q^0 = 1600$ MeV for $T = 0$ to a more diffused form at higher temperatures where it extends even below $q_0 = 1500$ MeV. First, we see from the left-hand panel of Fig. 2 that the in-medium $I = 0$ $\tilde{\Lambda}_c$ resonance becomes broadened and shifted to higher energies with increasing temperature. We note, however, that a single nucleon-hole state may be created at a higher energy for

higher T because the nuclear matter Fermi surface gets more diffused. In addition, at higher T , the nucleon single-particle potential becomes repulsive already at relatively low momenta. Hence, the resulting $\tilde{\Lambda}_c N^{-1}$ configuration which dictates the D spectral strength may spread eventually to lower energies as well with increasing temperature. So from what we see in Fig. 4, along with the wide collision broadening of the quasiparticle structure of D , this particle-hole structure as seen in the D spectral function might well kinematically facilitate the decay process $J/\Psi N \rightarrow \tilde{\Lambda}_c \bar{D}$ in a dense nuclear matter at finite temperature, say, in high energy heavy-ion collisions. This should of course depend on how the \bar{D} meson may behave in the same nuclear matter environment, which we are studying below.

3.2 \bar{D} meson in nuclear matter

With our models A and B introduced in Sect. 2, we are able to study the properties of the \bar{D} meson in a hot and dense nuclear matter. In fact, as found in Subsect. 2.2, this case is far easier to deal with because the $\bar{D}N$ equation is a single-channel one for both $I = 0$ and 1 isospin channels. Furthermore, the T-W vector interaction in the $I = 0$ channel has a strictly *vanishing* interaction strength, so the model B interaction produces no contribution in this isospin channel. In other words, the non-vanishing $I = 0$ channel contribution in the $\bar{D}N$ channel comes entirely from the spin-isospin singlet Σ_{DN} contribution in model A. The only available work to date on the \bar{D} in nuclear matter is found in Ref. [24] for the case of zero ($T = 0$) temperature, with which we may compare our results.

We first present in Table 1 results for the effective $\bar{D}N$ interaction in free space. In particular, we show the $I = 0$ and $I = 1$ scattering lengths defined as

$$a_{\bar{D}N} = -\frac{1}{4\pi} \frac{M_{\bar{D}N}}{\sqrt{s}} T_{\bar{D}N \rightarrow \bar{D}N} \quad (20)$$

at $\bar{D}N$ threshold, where $M_{\bar{D}N}$ is the total mass of the $\bar{D}N$ system. We use three different models which will be discussed in the following. The result from model A and B may not need any special explanation in view of what has been stated so far in the present subsection. However, we want to reiterate that the $I = 0$ contribution in model A is entirely from the Σ_{DN} contribution. Upon comparing these results with those from Ref. [24]: $a_{I=1}^{LK} = -0.26$ fm, and $a_{I=0}^{LK} = -0.16$ fm, we see immediately that while the $I = 1$ value is very close, there is a disagreement in the $I = 0$ scattering length. In an attempt to clarify this discrepancy we have adopted a dimensional regularization method (DR) which was used in [24], but with some minor modification in the subtraction point as well as in the form of the interaction of [23], as discussed in [17]. The results, presented as the “DR” entries in Table 1, are very close to the cut-off model B values, which is what one should have anticipated given the fact that the modifications implemented in Ref. [17] alter the original form of the Hofmann-Lutz T-W interaction [24] and the unitarization of the amplitude only marginally, especially in the present $\bar{D}N$ channel. Note also that in our DR approach the value of the meson decay constant has been chosen to be $f = f_\pi$ as compared with $1.15f_\pi$ in models A and B. The $I = 0$ scattering length turns out as, of course, zero,

Table 1: $\bar{D}N$ scattering lengths (fm)

	model A	model B	DR
$I = 0$	0.61	0	0
(Born approx.)	(0.26)	(0)	(0)
$I = 1$	-0.26	-0.29	-0.24
(Born approx.)	(-0.61)	(-0.88)	(-1.16)

with the vanishing interaction strength. So the $a_{I=0}^{LK}$ value quoted in Ref. [24] remains to be somewhat puzzling to us.

A recent calculation of Haidenbauer and collaborators [41] employs a meson-exchange approach supplemented by a short-range one-gluon exchange (OGE) contribution. It presents a similar $I = 0$ scattering length ($a_{I=0}^H = -0.07$ fm) but the $I = 1$ one is repulsive and almost twice our result ($a_{I=1}^H = -0.45$ fm). Since the OGE mechanism has no counterpart within our model, the comparison of results may not be very meaningful at this point. Nevertheless, it is worth noticing that about half of the repulsive scattering length $a_{I=1}^H$ comes from the hadronic meson-exchange contributions, which can be mapped to a certain extent to the T-W interaction used in the present work.

To see whether the interaction is reasonably weak, hence the Born approximation be appropriate or not, we have also calculated the scattering lengths in that approximation as shown in the table. We find a big discrepancy between the exact and approximate values, thus concluding that one has to sum up the whole iterative series even for this apparently smooth $\bar{D}N$ interaction as noted also in Ref. [41]. Thus the Born approximation is not adequate in studying the in-medium \bar{D} either. Note that, in the Born approximation, the $I = 1$ scattering length is less repulsive in model A due to the attractive contribution of the spin-isospin singlet Σ_{DN} term, while the scattering lengths calculated from the fully iterated amplitude are very similar in both models. Taking the isospin-averaged scattering length from the results in Table 1, one establishes a repulsive nature for the $\bar{D}N$ interaction, even in model A which contains the attractive effect of the Σ_{DN} term.

The \bar{D} optical potential in the nuclear medium may be defined as,

$$U_{\bar{D}}(\vec{q}) = \frac{\Pi_{\bar{D}}(E_{qp}(\vec{q}), \vec{q})}{2\sqrt{m_{\bar{D}}^2 + \vec{q}^2}} \quad (21)$$

and, at zero momentum, it can be identified as the in-medium shift of the \bar{D} meson mass. Our results for the \bar{D} mass shift are displayed in Fig. 5 in the case of model A (solid line) and B (dot-dashed line) including the MFB for nucleons.

The inclusion of an attractive Σ_{DN} term in model A gives rise to a less repulsive mass shift at $\rho = \rho_0$, of 11 MeV, in contrast to the 20 MeV repulsion found for model B. The absence of resonant states close to threshold in this $\bar{D}N$ scattering problem suggests extending the validity of the low-density theorem to normal nuclear matter densities or beyond. However, the low-density or $T\rho$ results, obtained by replacing the medium-dependent amplitude by the free-space one and displayed by the dashed and dotted lines

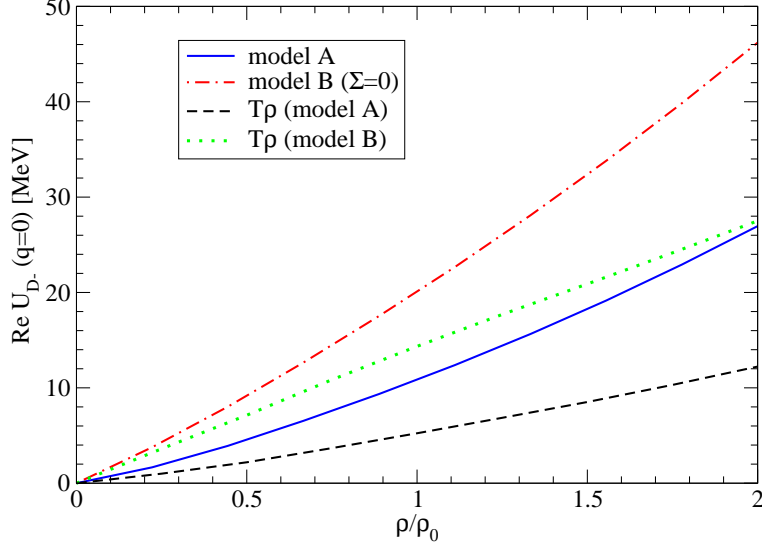


Figure 5: The \bar{D} mass shift in model A and B ($\Sigma_{DN} = 0$) including the MFB for nucleons as well as the low-density approximation as a function of density.

for models A and B, respectively, deviate quite substantially from the corresponding fully self-consistent results at a relatively low value of nuclear matter density. The additional sources of density dependence present in a full calculation can also be visualized by the deviation of the solid and dot-dashed lines from a linear behavior. At normal nuclear matter density, the low-density mass shift for model B is 15 MeV, while the fully-self-consistent result increases this value to 20 MeV. The same difference of about 5 MeV between the mass shifts obtained in both approaches is found for model A, as can be seen in Fig. 5. Our mass shift of 20 MeV at ρ_0 for model B is similar to the one in Ref. [24] within 10%.

3.3 In-medium D and \bar{D} optical potentials at finite temperature

In this last subsection we compare in Fig. 6 the D and \bar{D} optical potentials at $q = 0$ MeV/c as functions of temperature for two different densities (ρ_0 and $2\rho_0$) and for models A and B. The D meson potential is calculated self-consistently with MFB on baryons and with PD, and the \bar{D} meson is obtained also in a self-consistent manner only with MFB, since pion dressing does not enter here. The mass shift for D and \bar{D} mesons is reduced with temperature since, as observed for the spectral functions in Fig. 4, the quasiparticle peak moves towards the free position. This effect was also observed previously in Ref. [22] and it is due to the reduction of the self-energy as temperature increases because the meson-baryon interaction is averaged over larger momentum components where it is weaker. For model A (B) and at $T = 0$, we obtain an attractive potential of -12 (-18) MeV for D meson while the repulsion for \bar{D} is 11 (20) MeV. A similar shift in the mass for D mesons is obtained in Ref. [22]. The imaginary part and, hence, the width of the spectral function

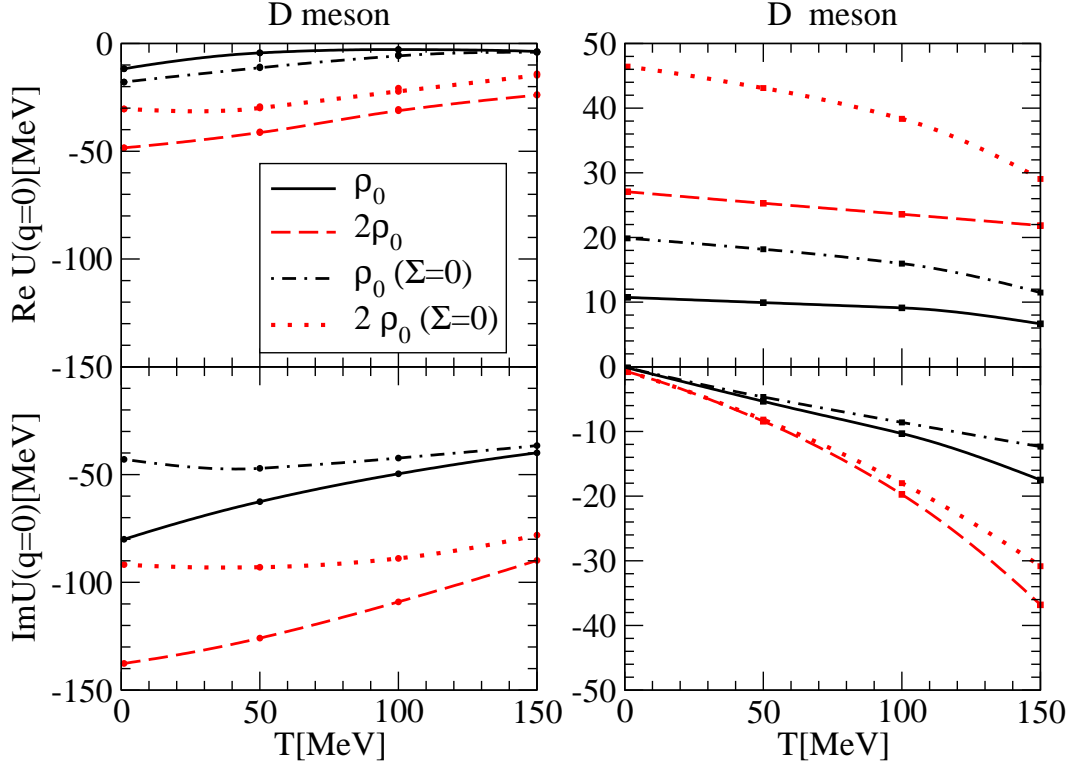


Figure 6: The D and \bar{D} potentials for the full selfconsistent calculation at $q = 0$ MeV/c for ρ_0 and $2\rho_0$ in models A and B ($\Sigma_{DN} = 0$) as a function of temperature.

for the quasiparticle tends to increase slightly with temperature for \bar{D} mesons due to the increase in the collisional width, while for D mesons it is somewhat reduced. Note, however, the different energy scales used in the D and \bar{D} plots. In fact, the situation is more involved for D mesons. On the one hand, the collisional width due to $DN \rightarrow DN$ processes also increases with temperature, but at low T the D meson width is largely dominated by the mixing of the quasiparticle peak to the $\tilde{\Sigma}_c N^{-1}$ components of the D meson self-energy. This is also the reason why the quasiparticle peak is located at a lower energy for model B, contrary to what one expects, as explained in the subsequent paragraph below. As T increases, the $\tilde{\Sigma}_c$ resonance gets diluted and, correspondingly, the width decreases. It is expected, however, that the width will eventually increase with T when it becomes mostly of collisional origin at high enough temperatures.

With regard to the effect of the Σ_{DN} term, we find that, for \bar{D} mesons, its inclusion substantially reduces the repulsion, independently of the temperature and density, since the dominant repulsive $I = 1$ scattering length is partly compensated by the attractive $I = 0$ one. However, this simple picture can not be applied to the D meson due to the presence of the $I = 1$ $\tilde{\Sigma}_c$ close to the DN threshold. We see that, in this case, there is a crossover when we go from ρ_0 to $2\rho_0$. The inclusion of the Σ_{DN} term alters the position of

the $\tilde{\Sigma}_c$ close to the DN threshold (as seen in Fig. 2). Therefore, while it has the expected attractive effect to the real part of the potential at $2\rho_0$, it effectively induces a repulsive effect for ρ_0 . The imaginary part increases with the inclusion of Σ_{DN} term for both mesons.

4 Summary and Conclusions

We have performed a hadronic self-consistent coupled-channel calculation of the D and \bar{D} self-energies in symmetric nuclear matter at finite temperature taking an effective meson-baryon Lagrangian that combines the charmed meson degree of freedom in a consistent manner with the chiral unitary models. This interaction consists of a broken s -wave SU(4) Tomozawa-Weinberg (T-W) contribution supplemented by a scalar-isoscalar Σ_{DN} term interaction. The corresponding in-medium solution at finite temperature obtains the dressing of $D(\bar{D})$ by Pauli blocking effects, dressing of π (PD), and the nuclear mean field binding effect (MFB) not only on the nucleons, but also on the charmed and strange hyperons by a finite-temperature σ - ω mean-field calculation.

In nuclear matter at $T = 0$, the dynamically generated $I = 0$ $\tilde{\Lambda}_c$ and $I = 1$ $\tilde{\Sigma}_c$ resonances in the $C = 1$ charm sector lie around 40 MeV below their free space values. Also at $T = 0$, the baryon binding results in an attractive mass shift for those resonances as compared to the case with no such effect. But, as we incorporate finite temperature, those resonances tend to move back to their free position acquiring a remarkable width due to the smearing of the Fermi surface.

The $\tilde{\Lambda}_c$ and $\tilde{\Sigma}_c$ resonances induce resonant-hole excitation modes that are clearly seen in the low-temperature D meson spectral function. The width of the distribution in fact reflects the overlap of the quasiparticle peak with the $\tilde{\Sigma}_c N^{-1}$ components of the D meson self-energy. As temperature increases, these modes tend to smear out and the D meson spectral function becomes a single pronounced quasiparticle peak close to the free D meson mass with fairly extended tails, particularly to the lower energy side of the distribution. At high temperature the width of the quasiparticle peak gets reduced slightly, so most of the distribution of the spectral function concentrates around the quasiparticle energy, although maintaining the overall strength in its lower energy part. As density increases, the quasiparticle peak broadens and the low-energy strength, associated to the $\tilde{\Lambda}_c N^{-1}$ components and related to $Y_c \pi N^{-1}$, $Y_c N N^{-2}$, ... absorption modes, obviously increases.

In the $\bar{D}N$ sector, we have first obtained the free space $I = 0$ and $I = 1$ scattering lengths. While our repulsive $I = 1$ value of $a_{I=1} \sim -0.3$ fm is in good agreement with Lutz and Korpa results [24], the finite value for the $I = 0$ scattering length found in this latter reference is in contrast to the zero value found here for model B due to the vanishing $I = 0$ coupling coefficient of the corresponding pure Tomozawa-Weinberg $\bar{D}N$ interaction. Our results are, however, consistent with a recent calculation based on a meson-exchange model supplemented by a short-range one-gluon exchange contribution [41]. For model A, we obtain a non-zero value of the $I = 0$ scattering length, dictated entirely by the magnitude of the Σ_{DN} term, which takes a rather conservative value in our present work. We have also observed that, in spite of the weakness of the $\bar{D}N$ interaction and the absence

of resonances close to threshold, the Born approximation is not sufficient to describe the free-space $\bar{D}N$ interaction at low energies.

As for medium effects, they induce a repulsive shift in the \bar{D} meson mass of 11 MeV (20 MeV) for model A (B) in nuclear matter at saturation density. Although the medium modifications of the $\bar{D}N$ interaction are more moderate than in the case of DN , we observe that the low-density approximation breaks down at relatively low densities. At nuclear matter saturation density, the \bar{D} meson mass shifts obtained from a fully self-consistent calculation are 5 MeV larger than those of the low-density approximation. The temperature dependence of the repulsive real part of the \bar{D} optical potential is very weak, while the imaginary part increases steadily due to the increase of collisional width. The picture is somewhat different for the D meson. At low temperature, the corresponding quasiparticle peak is already quite broad due to the overlap with the $\tilde{\Sigma}_c N^{-1}$ mode. As temperature increases the later mode tends to dissolve and, with the overlap being reduced, one observes an overall decrease in the width of the distribution in spite of the increase of collisional broadening.

Taking into account our results, we might look at the question of possible \bar{D} bound states once discussed in [13]. While D^- -mesic nuclei systems will always be bound by the Coulomb interaction, it would be interesting to see whether strongly bound nuclear states or even bound \bar{D}^0 nuclear systems might exist. From the results of Fig. 5 we see that, even for model A, the \bar{D} -nucleus optical potential at zero momentum is repulsive, hence ruling out this possibility. However, as mentioned earlier, the Σ_{DN} term, which contributes attractively to both isospin channels of the $\bar{D}N$ interaction, has been given a conservative value in our present approach. Although the magnitude of the Σ_{DN} term may be made larger, we recall that it is not a free parameter but is constrained by the coupled DN channel, in particular by the properties of the $\Lambda_c(2593)$ resonance. Therefore, it will be first necessary to see whether a larger Σ_{DN} term constrained by the properties of the DN interaction may still produce an attractive isospin averaged interaction, which could then even allow for the existence of \bar{D}^0 -nucleus bound states. In any event, it is clear that D^- -mesic nuclei provide a valuable source of information for determining the sign and size of the \bar{D} mass shift at subnuclear densities. An experimental observation of bound D nuclear states is ruled out by the large width and moderate attraction found for the D meson optical potential.

The other point of interest from the present study is related to the possible hadronic mechanism for the suppression of the J/Ψ production in relativistic heavy-ion collisions. As stated in the introduction, a good part of the earlier interest was to see if the masses of D and \bar{D} get reduced so that the $J/\Psi \rightarrow D\bar{D}$ may proceed *exothermically* [13,14,16,24] in nuclear matter, hence contributing to the J/Ψ suppression. The difference in the two thresholds in vacuo for this process is $\Delta E \equiv E_{th}(D + \bar{D}) - E_{th}(J/\Psi) \approx 650$ MeV, which should be overcome in one way or another for this to go spontaneously or at the cost of small energies. Since charmonia including the J/Ψ are $c\bar{c}$ bound states which do not contain any light quarks, one normally assumes that the medium modification they might undergo should be minimum, thus their in-medium masses are not expected to be very different from those in vacuo. In the present work, we have observed that in-medium \bar{D} mass

increases typically by 10 – 20 MeV. On the other hand, as mentioned in the last section, from Fig. 4, the tail of the quasiparticle peak of the D spectral function extends with a non-negligible strength to lower “mass” values due to the thermally spread $\tilde{Y}_c N^{-1}$ particle-hole configurations. So one might expect that some spontaneous leakage for $J/\Psi N \rightarrow \tilde{Y}_c \bar{D} \rightarrow Y_c \pi \bar{D}$, $J/\Psi NN \rightarrow Y_c N \bar{D}$, ... might effectively be possible. However, it looks very unlikely that the lower part of this spectral function tail extends from the quasiparticle peak as far down by 600 MeV while keeping relevant strengths. So the disappearance of the J/Ψ through such processes, even if helped by the thermally excited nucleons, will not proceed. These processes might still go endothermically through collisions induced by a surrounding large collection of co-moving hadrons for which the effective reaction threshold may get lowered. But its efficiency is very questionable. So the direct disappearance of the existing J/Ψ looks improbable.

Then, what about the possibility of reducing the supply of this charmonium from its excited state partners such as $\chi_{c\ell}(1P)$, ($\ell = 0, 1, 2$) since it is known that an appreciable fraction of J/Ψ production comes from the radiative decay of these charmonia [42]? To look for such a possibility, we may consider here the following reactions: $\chi_{c\ell}(1P)N \rightarrow \Lambda_c(2285)\bar{D}$, $\chi_{c\ell}(1P)N \rightarrow \Lambda_c(2285)\pi\bar{D}$, $\chi_{c\ell}(1P)N \rightarrow \Sigma_c(2445)\bar{D}$ and $\chi_{c\ell}(1P)N \rightarrow \tilde{\Lambda}_c(2593)\bar{D}$. Note that the masses of these $\chi_{c\ell}$ ’s are 3415, 3511, and 3556 MeV in ascending order for ℓ . Before proceeding, we note that in free space the first three reactions are already endothermic for all three $\chi_{c\ell}$ ’s, while the last one is closed for the two lowest ones. Upon taking into account the MFB effects studied in the present work, it should be safe to speculate that the same first three reactions do take place in a hot nuclear matter as well. As for the last one, we might also claim that it could proceed in medium since the $\tilde{\Lambda}_c$ will develop a sufficient width as seen, for example, in the in-medium DN amplitudes of Fig. 2 or reflected in the extended low energy tail of the D meson spectral functions in Fig. 4. Therefore part of the feeding of the J/Ψ from its excited state partners will certainly be reduced. A similar mechanism might well reduce the feeding of J/Ψ from the decay of the Ψ' . The arguments presented here are only kinematical in nature, so even a simple dynamical model for the relevant in-medium reactions may need to be employed to support them further.

5 Acknowledgments

T.M. is grateful to the support offered through the host (A.R) for his stay in Barcelona, and for part of his travel. This work is partly supported by the EU contract FLAVIANet MRTN-CT-2006-035482, by the contract FIS2005-03142 from MEC (Spain) and FEDER and by the Generalitat de Catalunya contract 2005SGR-00343. This research is part of the EU Integrated Infrastructure Initiative Hadron Physics Project under contract number RII3-CT-2004-506078. L.T. wishes to acknowledge support from the BMBF project “Hadronisierung des QGP und dynamik von hadronen mit charm quarks” (ANBest-P and BNBest-BMBF 98/NKBF98).

References

- [1] T. Matsui and H. Satz, Phys. Lett. B **178**, 416 (1986)
- [2] M. Gonin *et al.* [NA50 Collaboration], Nucl Phys. A **610**, 404c (1996)
- [3] L. Lammello *et al.* [NA50 Collaboration], Nucl. Phys. A **638**, 261c (1998); M.C. Abreu *et al.*, Phys. Lett. B **450**, 456 (1999)
- [4] M.C. Abreu *et al.*, Eur. Phys. J. C **14**, 443 (2000)
- [5] R. Arnaldi *et al.* [NA60 Collaboration], J. Phys. G **32**, S51 (2006)
- [6] A. Adare *et al.* [PHENIX Collaboration], Phys. Rev. Lett. **98**, 232301 (2007); T. Gunji [PHENIX Collaboration], J. Phys. G **34**, S749 (2007)
- [7] Y. Aoki, Z. Fodor, S.D. Katz and K. K. Szabo, Phys. Lett. B **643**, 46 (2006)
- [8] Z. Fodor and S. D. Katz, Journ. High Ener. Phys. **04**, 050 (2004)
- [9] C. Ratti, M. A. Thaler and W. Weise, Phys. Rev. D **73**, 014019 (2006)
- [10] K. Tsushima, A. Sibirtsev, K. Saito, A. W. Thomas and D. H. Landau, Nucl. Phys. A **680**, 280 (2001)
- [11] W. Cassing, E.L. Bratkovskaya and A. Sibirtsev, Nucl. Phys. A **691**, 753 (2001)
- [12] R. Shahoyan [NA60 Collaboration], J. Phys. G **34**, S1029 (2007)
- [13] K. Tsushima, D.H. Lu, A.W. Thomas, K. Saito and R.H. Landau, Phys. Rev. C **59**, 2824 (1999)
- [14] A. Sibirtsev, K. Tsushima and A.W. Thomas, Eur. Phys. J. A **6**, 351 (1999)
- [15] A. Hayashigaki, Phys. Lett. B **487**, 96 (2000)
- [16] A. Mishra, E.L. Bratkovskaya, J. Schaffner-Bielich, S. Schramm and H. Stöcker, Phys. Rev. C **70**, 044904 (2004)
- [17] T. Mizutani and A. Ramos, Phys. Rev C **74**, 065201 (2006)
- [18] M. Gazdzicki and M. Gorenstein, Phys. Rev. Lett. **83**, 4009 (1999)
- [19] M. Gazdzicki, Phys. Rev. C **60**, 054903 (1999)
- [20] K. Gallmeister, B. Kämpfer and O.P. Pavlenko, Phys. Lett. B **473**, 20 (2000)
- [21] L. Tolos, J. Schaffner-Bielich and A. Mishra, Phys. Rev. C **70**, 025203 (2004)
- [22] L. Tolos, J. Schaffner-Bielich and H. Stöcker, Phys. Lett. B **635**, 85 (2006)

- [23] J. Hofmann and M.F.M. Lutz, Nucl. Phys. A **763**, 90 (2005)
- [24] M.F.M. Lutz and C.L. Korpa, Phys. Lett. B **633**, 43 (2006)
- [25] J. Oller and U.G. Meissner, Phys. Lett. B **500**, 263 (2001)
- [26] E. Oset and A. Ramos, Nucl. Phys. A **635**, 99 (1998)
- [27] A. Ramos and E. Oset, Nucl. Phys. A **671**, 481 (2000)
- [28] L. Tolos, A. Ramos and E. Oset, Phys. Rev. C **74**, 015203 (2006)
- [29] T. Maruyama, T. Muto, T. Tatsumi, K. Tsushima and A.W. Thomas, Nucl. Phys. A **760**, 319 (2005)
- [30] M. Artuso *et al.* [CLEO collaboration], Phys. Rev. Lett. **95**, 251801 (2005)
- [31] W.M. Yao *et al.* [Particle Data Group], J. Phys. G **33**, 1 (2006).
- [32] J.I. Kapusta and C. Gale, *Finite Temperature Field Theory Principles and Applications*, 2nd. edition (Cambridge Univ. Press, 2006)
- [33] R. Machleidt, Adv. Nucl. Phys. **19**, 189 (1989)
- [34] K. Tsushima and F.C. Khanna, Phys. Lett. B **552**, 138 (2003); K. Tsushima and F.C. Khanna, J. Phys. G **30**, 1765 (2004)
- [35] L. Tolos, A. Ramos and A. Polls, Phys. Rev. C **65**, 054907 (2002)
- [36] E. Oset, P. Fernandez de Cordoba, L.L. Salcedo and R. Brockmann, Phys. Rep. **188**, 79 (1990)
- [37] A. Ramos, E. Oset and L.L. Salcedo, Phys. Rev. C **50**, 2314 (1994)
- [38] R. Seki and K. Masutani, Phys. Rev. C **27**, 2799 (1983); O. Meirav, E. Friedman, R.R. Johnson, R. Olszewski and P. Weber, Phys. Rev. C **40**, 843 (1989)
- [39] E. Oset, H. Toki and W. Weise, Phys. Rep. **83**, 28 (1982)
- [40] L. Tolos, D. Cabrera, A. Ramos and A. Polls, Phys. Lett. B **632**, 219 (2006); and references herein.
- [41] J. Haidenbauer, G. Krein, U.G. Meissner and A. Sibirtsev, Eur. Phys. J. A **33**, 107 (2007)
- [42] L. Antoniazzi *et al.* [E705 Collaboration], Phys. Rev. Lett **70**, 383 (1993)